Postharvest Biology and Technology 225 (2025) 113520

Contents lists available at ScienceDirect

Postharvest Biology and Technology

journal homepage: www.elsevier.com/locate/postharvbio

Investigating apple surface condensation and mass loss with IoT and predictive modelling

Akshay D. Sonawane [a,*], Tuany G. Hoffmann [a], Reiner Jedermann [b], Manfred Linke [a], Pramod V. Mahajan [a,*]

[a] Department of Systems Process Engineering, Leibniz Institute for Agricultural Engineering and Bioeconomy (ATB), Potsdam, Germany
[b] Institute for Microsensors, -actuators and -systems (IMSAS), University of Bremen, Bremen 28359, Germany

ARTICLE INFO

Keywords:
Apple storage
Respiration
Transpiration
Raspberry Pi
Kafka
Digital twin

ABSTRACT

This study analysed condensation and mass loss in apple storage using an IoT system and predictive modelling. A condensation model, based on the mass transfer coefficient determined through the Sherwood number for the relation between convective and diffusive mass transfer, and a mass loss model incorporating transpiration and respiration, were developed to predict cumulative condensation, retention time, cumulative mass loss, and at the end, the total mass of apples in storage. The model was validated with individual and bulk apples kept under varying air temperature conditions. Data on air and surface temperature, humidity, air speed, and surface wetness were collected via sensors, processed through Raspberry Pi (embedded computer) and Kafka data streaming platform for predictions, and stored in the InfluxDB time-series database for visualisation. The real-time model predictions were effectively aligned with experimental trends. In individual apple trials, 45- and 60-minute on-off refrigeration cycles showed the predicted peak cumulative condensations of 0.05 and 0.12 g kg^{-1}, approximately 71 % and 77 % of experimental peaks, with mass losses of 0.27 and 0.24 g kg^{-1} over 12 hours, respectively. In bulk apple trials, predicted peaks were 0.03 and 1.03 g kg^{-1}, around 30 % and 58 % of experimental values, with mass losses of 0.96 and 0.82 g kg^{-1} over 60 hours for low and high-temperature fluctuations, respectively. Temperature fluctuations significantly influenced condensation and mass loss, with high fluctuations causing much greater cumulative condensation than low fluctuations. However, experimental peak cumulative condensation values were consistently higher than predicted ones, likely due to the accuracy of sensors, the complexity of the experimental setup, and theoretical model assumptions. Transpiration accounted for a larger portion of the total cumulative mass loss in apples compared to respiration. Additionally, longer condensation retention times resulted in reduced apple mass loss.

1. Introduction

Condensation occurs when water vapour in moist air comes in contact with cooler surfaces and water vapour condenses into liquid. This process is closely related to the dew point temperature which is the temperature at which air becomes fully saturated (100 % relative humidity) and water vapour begins to condense within fruit packaging (Bovi et al., 2016; Jalali et al., 2020; Linke and Geyer, 2013) and storage environments (Linke et al., 2023). If condensation remains on the fruit surface, it can facilitate the growth of microorganisms, leading to changes in colour, texture, and flavour, and accelerating spoilage (Wei et al., 1998; Li et al., 2022). Fungal pathogens like *Penicillium* spp., *Botrytis* spp., and others thrive under high humidity, reducing shelf life (Chen et al., 2023). Although, the condensation can also act as a protective barrier, reducing transpiration and helping fruits retain moisture, turgidity, and freshness (Linke et al., 2021), its role in causing diseases (Gray mould, blue mould, Rhizopus rot, bacterial soft rot, and acid rot) is more significant than its benefits in reducing transpiration.

Several studies have investigated condensation dynamics in fruit storage environments, developing models based on key input variables such as fruit surface temperature, airflow, air temperature, and relative humidity. However, these models are standalone and do not incorporate real-time predictive capabilities. Gottschalk et al. (2007) developed a model that represents the condensation and evaporation processes on a plum. The model prediction matched with an experimental condensation amount of ~0.3 g for plum mass of 188 g at 19.5°C of ambient air

* Corresponding authors.
E-mail addresses: ASonawane@atb-potsdam.de (A.D. Sonawane), PMahajan@atb-potsdam.de (P.V. Mahajan).

https://doi.org/10.1016/j.postharvbio.2025.113520
Received 13 December 2024; Received in revised form 11 March 2025; Accepted 12 March 2025
Available online 21 March 2025
0925-5214/© 2025 The Author(s). Published by Elsevier B.V. This is an open access article under the CC BY license (http://creativecommons.org/licenses/by/4.0/).

with 60 % relative humidity. Linke et al. (2021) used a wetness sensor to measure condensation retention time on apples and validated it through continuous weighing and dew-point measurements. Experimental condensation on a 191.8 g apple peaked at 40 mg at 21.8°C and 62.0 % relative humidity. In a separate investigation, Linke et al. (2023) assessed the presence of condensation varied between 33.4 % and 100 % during cooling and warming cycles, depending on the system settings, highlighting the impact of refrigeration system on condensation in storage. Lequentrec et al. (2023) studied condensation on an orange (~0.40 g) during warming (~25°C, 60 % humidity) and cooling (4°C, 80–90 % humidity) phases. Airflow at 0.33 m s^{-1} caused uneven condensation and evaporation.

Mass loss in fruit is primarily driven by transpiration and respiration, with varying contributions depending on the species and variety of fruit, storage conditions, and other environmental factors. In the process of transpiration, the water evaporates from the surface of the fruit, which accounts for over 90 % of mass loss in fresh produce under typical storage conditions (Lufu et al., 2019). Water loss is influenced by internal factors such as the fruit's volume, size, surface characteristics (including stomata, lenticels, and cuticle), any damage to the fruit, and the boundary layer around it. External factors include airflow, temperature, relative humidity, and vapour pressure deficit (VPD) (Bovi et al., 2019). Respiratory processes, though less significant, also contribute to mass loss by consuming sugars and releasing water vapour and carbon dioxide during the metabolism of stored energy (Jalali et al., 2020). Advanced models for simulating mass loss incorporate factors such as fruit structure, environmental conditions, and physiological responses. A biophysical model simulates water relations and fruit growth dynamics, helping to predict changes in fruit mass during storage. Apples can lose from 3.5 (*Jonagold*) to 4.1 % (*Elstar*) of total mass loss depending on variety during six months of storage at 97.5 % relative humidity (Veraverbeke et al., 2003a; Veraverbeke et al., 2003b).

In recent years, the Internet of Things (IoT) has opened up exciting possibilities, enabling interconnected devices to collect data from their domain and predict physical quantities in the post-harvest supply chain (Huang et al., 2023). This emerging IoT field can present opportunities for predicting and managing environmental factors affecting perishable fruit, including condensation and mass loss (Kasera et al., 2024). The real-time IoT system can easily integrated with a digital twin platform to optimise the supply chain and storage conditions of fresh produce (Defraeye et al., 2021; Shoji et al., 2022).

Apples are typically stored in long-term cold storage at 1–4°C and 95 % relative humidity (Paull, 1999). Temperature fluctuations in cold storage, caused by refrigeration system cycles, lead to condensation on apple surfaces and mass loss from apples (Vicent et al., 2018; Praeger et al., 2021). Only a few studies have explored the use of IoT technology to monitor storage conditions (temperature, relative humidity, and airflow) in apple cold storage. Jedermann et al. (2018) investigated the performance of sub-GHz wireless communication for IoT-based sensor monitoring in apple cold storage. It demonstrated that LoRa and industrial radio frequency modules at 866 MHz ensured reliable data transmission while measuring product temperature and local airflow inside the storage. However, to our knowledge, no existing research combines models for condensation on fruit surfaces and mass loss with real-time IoT-based predictions. Therefore, the aim of this study was twofold: first, to develop an IoT-driven predictive model for both condensation occurrence on apple surface and mass loss over time; and second, to validate this model by comparing its predictions with experimental measurements of condensation and mass loss. Overall, integrating these models into storage and transport systems could improve predictions for mass loss and optimise conditions to minimise mass loss reduction, ultimately maintaining fruit quality during storage.

2. Model development

2.1. Model for condensation on fruit surface

To determine the amount of condensation on the surface of fruit, the mass transfer coefficient plays a critical role. The mass transfer coefficient is a parameter that quantifies the rate at which mass, such as water vapour, moves between the surface of the fruit and the surrounding air. It depends on various factors such as airflow, temperature gradients, and surface properties. By multiplying the mass transfer coefficient with the time difference, the volume-related water content difference between the surface of the fruit and the air, and the surface area of the fruit, the mass of condensed water can be estimated. The stepwise explanation for determining the amount of condensation on the surface of fruit is outlined below.

To calculate the volume-based water content of air at the fruit surface and in the surrounding air, the saturation and actual vapour pressures for each respective region must first be calculated. The saturation pressure of water vapour in the air and at the fruit surface at temperature T_{air} and $T_{surface}$ is calculated using the following improved Magnus formula (Huang, 2018).

$$Psat_{air/surface} = 610.64 \exp\left(\frac{17.625\, T_{air/surface}}{243.04 + T_{air/surface}}\right) \tag{1}$$

Where Psat is the saturated water vapour pressure with subscripts used for air and fruit surface in Pa, and T is the respective temperature in °C with subscripts for air and surface. The actual water vapour pressure (P_{air}) is calculated by multiplying $Psat_{air}$ by the relative humidity of the air (RH_{air}) as shown below:

$$P_{air} = \frac{Psat_{air}\, RH_{air}}{100} \tag{2}$$

In psychrometric principles, absolute humidity provides a direct measure of how much moisture is present in the air. It is useful for understanding the capacity of air to hold water vapour at different temperatures, as warmer air can hold more moisture than cooler air. The water content of ambient air is given by the following formulae (Linke et al., 2024).

$$x_{air} = \frac{(R_{air} / R_{wv})\, P_{air}}{(P - P_{air})} \tag{3}$$

$$\rho_{air} = \frac{(1 + x_{air})\, P_{air}}{((R_{air} / R_{wv}) + x_{air})\, T_{air}} \tag{4}$$

$$Mwv_{air} = 1000\, x_{air}\, \rho_{air} \tag{5}$$

Where R_{air} is the gas constant of dry air (287.05 J kg^{-1} K^{-1}); R_{wv} is the gas constant of water vapour in the air (461.50 J kg^{-1} K^{-1}); P is total atmospheric pressure (101325 Pa); X_{air} is the mass related water content of the air in kg kg^{-1}; ρ_a is the density of moist air in kg m^{-3}; Mwv_{air} is the (volume-related) actual water content of the air in g m^{-3}. Similarly, the possible maximum water content ($Mwv_{surface}$) at the fruit surface (assuming 100 % relative humidity at the fruit surface) can be calculated using the above Eqs. (3 to 5), $T_{surface}$, and $Psat_{surface}$.

If the $T_{surface}$ falls below T_{dew}, condensation will occur on the fruit surface (Linke et al., 2023). The dew point temperature is calculated by using the Magnus-Tetens formula (Magnus, 1844).

$$T_{dew} = \frac{243.04\left(\ln\left(\frac{RH_{air}}{100}\right) + \frac{17.625\, T_{air}}{243.5 + T_{air}}\right)}{17.625 - \left(\ln\left(\frac{RH_{air}}{100}\right) + \frac{17.625\, T_{air}}{243.5 + T_{air}}\right)} \tag{6}$$

Where T_{dew} is the dew point temperature at T_{air} in °C and RH_{air} in %. In principle, $Mwv_{surface}$ falls below Mwv_{air}, so additional water ($Mwv_{air} - Mwv_{surface}$) will condense on the fruit surface. Therefore, the amount of

condensation in time dt (which is equal difference between current time t and previous time t-1) on the fruit is given by the following equation:

$$\frac{d}{dt}m_c = \left(Mwv_{air} - Mwv_{surface}\right) A_{surface} K_c \tag{7}$$

Where m_c is the amount of condensation in g calculated at time t; $A_{surface}$ is the surface area of fruit in m^2 and K_c is the mass transfer coefficient for condensation in m s^{-1}. The negative value of m_c represents the reverse process of condensation, known as evaporation. This value accounts for both the gain of water through condensation and the loss of water through evaporation over time on the fruit surface. This approach is particularly effective for fruits and vegetables with smooth surfaces, as these characteristics facilitate condensation. Examples of such produce include apples, pears, peaches, tomatoes, cucumbers, bell peppers, plums, etc. The cumulative value of $m_c(t)$ (denoted as $m_{ccum}(t)$) at time t, represents the total accumulated water condensation on the fruit's surface. This value is always non-negative, meaning it remains zero or greater at the end of each time step, as expressed in Eq. (8). If $m_c(t)$ is positive, condensation occurs on the surface of the fruit, leading to water formation. If $m_c(t)$ is negative, it indicates the evaporation of previously condensed water. However, once all condensed water has evaporated, further evaporation cannot occur even if $m_c(t)$ remains negative. At this point, transpiration (water loss from the fruit) begins instead. The equation governing cumulative condensation is:

$$m_{ccum}(t) = \frac{m_{ccum}(t-1) + m_c(t) + |m_{ccum}(t-1) + m_c(t)|}{2} \tag{8}$$

Where $m_{ccum}(t-1)$ is the non-negative cumulative condensation from the previous step.

The mass transfer coefficient for condensation (K_c) for condensation and evaporation can be calculated using the Sherwood number (Ramos et al., 2023).

$$K_c = \frac{Sh\, D_{wv}}{d} \tag{9}$$

Where Sh is Sherwood dimensionless number; d is the average diameter of fruit in m; D_{wv} is the diffusivity of water vapour in the air in m^2 s^{-1} and is calculated using the following equation (Montgomery, 1947):

$$D_{wv} = 2.26 \times 10^{-5} \left(\frac{(T_{air} + 273.15)}{273.15}\right)^{1.81} \tag{10}$$

The Nusselt number for heat transfer, as presented by Lequentrec et al. (2023), can be analogously applied to the Sherwood number for mass transfer. According to Incropera et al. (2007), this analogy involves substituting the Prandtl number (Pr) with the Schmidt number (Sc), reflecting the similar roles of these dimensionless numbers in their respective mass transport phenomena. Therefore, the resulting Sherwood number (Eq. (11)) gives the convective to diffusive mass transfer ratio in a manner analogous to heat transfer processes, accommodating the influence of fluid flow characterised by the Reynolds number (Re).

$$Sh = 2 + 1.3\, Sc^{0.15} + 0.66\, Sc^{0.31}\, Re^{0.50} \tag{11}$$

The numerical term 2 in Eq. (11) is a constant, representing the contribution of pure diffusion without the influence of flow or convection. The Reynolds and Schmidt numbers are calculated using Eqs. (12 and 13).

$$Re = \frac{\rho_{air}\, v\, d}{\mu_{air}} \tag{12}$$

$$Sc = \frac{\mu_{air}}{\rho_{air}\, D_{wv}} \tag{13}$$

where v is the speed of humid air in m s^{-1}; d is the average fruit diameter in m; μ_{air} is the dynamic viscosity of humid air in kg m^{-1} s^{-1} and D_{wv} is the diffusivity of water vapour in the air in m^2 s^{-1}. Eqs. (1 to 13) collectively constitute the model for describing condensation phenomena on fruit surfaces.

2.2. Model for mass loss of fruit

Minimising fruit mass loss is crucial in the post-harvest phase to maintain the freshness, nutritional value, and overall quality of fruit. Predictive modelling can reduce fruit mass loss by achieving optimised storage conditions. The mass loss in g from fruit due to the transpiration (m_{tr}) is given by the following equation (Becker et al., 1996):

$$\frac{d}{dt}m_{tr} = \begin{cases} 0, & \text{if } m_{ccum}(t) > 0 \\ \dfrac{(Psat_{surface} - P_{air})\quad 1000}{\dfrac{1}{K_s} + \dfrac{1}{K_c}} A_{surface}, & \text{if } m_{ccum}(t) = 0 \end{cases} \tag{14}$$

Where K_s is the skin mass transfer coefficient for transpiration in m s^{-1} and the mass transfer coefficient K_c, derived from previous condensation calculations, specifically pertains to the mass transfer occurring from the skin of the fruit to the ambient air when there is no condensate present on fruit surfaces. When condensation occurs on the surface of the fruit, there is ideally no transpiration mass loss from the fruit, meaning that the transpiration mass loss is effectively zero. In this scenario, only oxidative mass loss contributes to the reduction in fruit mass. The following model gives the oxidative mass loss (m_{oxi}) from fruit in g due to respiration (Jalali et al., 2021).

$$\frac{d}{dt}m_{oxi} = \begin{cases} n\,(m_{single})\, r_{CO2}\, \dfrac{180 - 108}{264}, & \text{if } t = 0 \\ m_{new}(t-1)\, r_{CO2}\, \dfrac{180 - 108}{264}, & \text{if } t > 0 \end{cases} \tag{15}$$

Where n is the number of apples; m_{single} is the initial average mass of a single apple in g; r_{CO2} is the CO_2 production rate of fruit in g kg^{-1} s^{-1}; $\frac{180-108}{264}$ is the conversion factor from the oxidation of glucose during respiration; $m_{initial}$ is the initial apple mass in g. Total mass loss is the sum of mass loss due to transpiration and mass loss due to respiration. The cumulative mass loss can be calculated using total mass loss like Eq. (8) but with the minimum function. Eqs. (14 and 15) collectively constitute the model for mass loss from fruit.

The new mass of the fruit is determined using a mass balance approach that accounts for various mass transfer processes affecting the fruit including condensation, mass loss due to respiration, and transpiration. The formula is expressed as:

$$m_{new}(t) = \begin{cases} n\,(m_{single}), & \text{if } t = 0 \\ m_{new}(t-1) + ((m_{ccum}(t) - m_{ccum}(t-1)) - m_{tr}(t) - m_{oxi}(t), & \text{if } t > 0 \end{cases} \tag{16}$$

Where $m_{new}(t)$ is the new mass of fruit in g including condensation and mass loss at time t; $m_{tr}(t)$ and $m_{oxi}(t)$ are the respective mass loss values at time t.

2.3. Numerical parameters and models for apple as a case study

To calculate condensation, transpiration mass loss, and oxidative mass loss for the apples, key values such as the surface area, mass transfer coefficient for moisture loss from the apple skin, and the respiration rate of the apples are required. These values can be obtained either through experimental measurements or sourced directly from existing literature. The surface area of apples in m^2 is calculated by using the formula (Clayton et al., 1995):

$$A_{surface} = n\left(0.0581\left(\frac{m_{single}}{1000}\right)^{0.685}\right)\varepsilon \tag{17}$$

Where ε represents a factor that accounts for the portion of the surface area lost due to touching in the total surface area. The calculated touching surface area in bulk was found experimentally to be 2 % of the total surface area of apples that were not in contact with each other, resulting in a value of $\varepsilon = 0.98$. The mass transfer coefficient for transpiration through the apple surface (cutin, wax, and cuticle) was experimentally determined as $2.30 \pm 0.19 \times 10^{-10}$ m s^{-1} at 5°C. The variation in this value can be negligible up to 10°C; therefore, it was assumed to remain constant from 0°C to 10°C. The average apple diameter was experimentally determined to be 6.5 ± 0.6 cm.

The r_{CO2} was determined to be 6.88×10^{-6} and 9.83×10^{-7} g kg^{-1} s^{-1} by Saquet and Streif (2017) for *Jonagold* apples at 20 and 0°C. Thus by applying the Arrhenius relationship for respiration rate, the following equation can predict the r_{CO2} at different temperatures.

$$r_{CO2} = 2.15 \times 10^6\, e^{-\frac{64486.44}{R\,(T_{air}+273.15)}} \tag{18}$$

Where R is the universal gas constant (8.314 J K^{-1} mol^{-1}); activation energy is 64486.44 J mol^{-1} and the pre-exponential factor is 2.15×10^6 g kg^{-1} s^{-1} in the Arrhenius relationship.

2.4. Numerical integration and computational details

The models for condensation and mass loss were integrated into a single model framework, implemented in Python using libraries such as *pandas*, *numpy*, *matplotlib*, *math*, *confluent_kafka*, *Adafruit_SHT45*, and *influxdb_client*. Numerical integration was performed explicitly, with time steps derived from input data timestamps, initialising the first step to zero (Sonawane et al., 2024). Standard 64-bit floating-point precision ensured accuracy. The model iteratively updated state variables, including fruit mass, condensation, mass loss, and retention time, using empirical and theoretical equations. Without relying on implicit solvers or adaptive time-stepping, the approach maintained straightforward and reproducible calculations, making it efficient for real-time applications. The developed computational model is provided as supplementary files, including the original Python code and its pdf.

3. Materials and methods

3.1. Experimental validation setup

A test was conducted to evaluate the performance of the developed condensation and mass loss model. The apples (variety: *Jonagold*; 1–2 months of storage after harvest) used for the experiment were purchased from a local supplier in Potsdam, Germany. The experimental validation was divided into two main sections. The first section, referred to as the individual apples, involved a small-scale experiment with three apples placed individually on a weighing balance. The second section called the bulk apples, focused on a large-scale experiment with a bulk quantity of apples placed in a box (length × width × height: 40 × 30 × 50 cm) on a weighing balance (Table 1 and Fig. 1). For the individual apple trials, a cooling chamber with a time-based on-off refrigeration cycle was used, while for the bulk apple experiment, the default temperature control system of the cooling chamber was applied with high and low-temperature fluctuations. Based on these setups, four trials were conducted to observe temperature fluctuations, as outlined in Table 1. Wet towels were placed in each chamber to maintain a relative

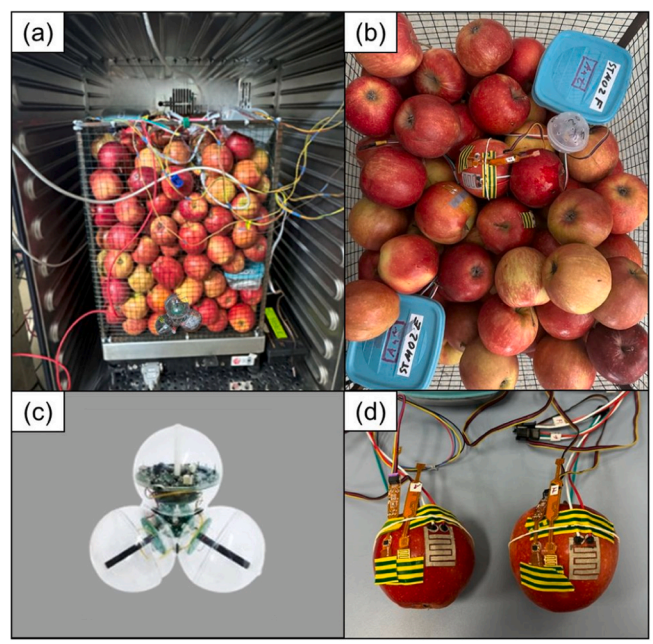

Fig. 1. (a) Bin filled with apples on a weighing balance in a cooling chamber; (b) Top view of the box during filling and sensor placement; (c) Air speed logger measuring cooling air speed in the box; (d) Wetness sensor (coil) and SHT45 for surface temperature (on apple), air temperature, and relative humidity.

Table 1
Experimental setup details for individual apple and bulk apple trials, including cooling chamber conditions, weighing balance specifications, and measurement parameters.

Experimental section	Trial number	Setup	Cooling chamber	Weighing balance	Measurements from cooling chambers
Individual apples	**#1** Periodic 45-minute on-off cycle over 12 hours (2.2–5.8°C) **#2** Periodic 45-minute on-off cycle over 12 hours (1.1–7.1°C)	Three apples (0.64–0.65 kg) placed on a weighing balance	BK6160 (Heraeus Deutschland GmbH & Co. KG, Germany)	CPA4202S (Sartorius, Germany) with a resolution of 1 mg	Air and apple surface temperature, and air relative humidity
Bulk apples	**#3** Low-temperature fluctuation cycle over 60 hours (4.2–6.3°C) **#4** High-temperature fluctuation cycle over 60 hours (2.7–8.3°C)	A single meshed box containing approximately 29 kg of apples placed on a weighing balance	Memmert IPP260 plus (Memmert GmbH + Co. KG, Germany)	LC16000S (Sartorius, Germany) with a resolution of 10 mg	Air and apple surface temperature, air relative humidity, air speed, and wetness signal

Table 2
Specifications and functions of electronics used for data collection and streaming.

Electronics	Function	Accuracy and range	Manufacturer and reference
Sensors:			
SHT45	To measure air, apple surface temperature and air relative humidity	± 0.10°C and ± 1.75 % relative humidity under cool chain conditions	Sensirion, Switzerland; Sensirion (2024)
Air speed logger	To measure cooling air speed	NA*	Geyer et al. (2018); Hoffmann et al., 2024
Wetness sensor	To measure the presence of condensate	NA*	Linke et al. (2021); Linke et al. (2023)
Microcontrollers and modules:			
STM32L031K6	To read inputs from multiple sensors and send them to Raspberry Pi	NA* *	STMicroelectronics, Switzerland; STMicroelectronics (2024)
Raspberry Pi (Model: 3B)	To receive data from up to STM32L031K6 microcontrollers via USB and transfer data wirelessly to Kafka	NA* *	Raspberry Pi Foundation, UK

*NA: Not available; * *NA: Not applicable.

humidity range of 70 to ~100 %.

In typical apple cold rooms, the maximum temperature fluctuation ranges from 0 to 4ºC. Selected temperature fluctuations, although not originally intended for apple cold storage rooms, were deliberately introduced to evaluate the performance of the developed IoT model in this study. These fluctuations could result in sufficient condensation and mass loss to test the predictive capabilities of the model.

All sensors used in this experiment are listed in Table 2 with their specifications. To measure air temperature, relative humidity, and air speed, sensors were strategically positioned within the void spaces between the apples. These sensors were placed approximately in the centre of the horizontal plane (40 × 30 cm) and deep inside the box, specifically in the middle to bottom section (below 25 cm from the top) along the vertical plane. For surface temperature and wetness of the apples, sensors were placed directly on the surface of the apples (Fig. 1). The sensors, along with the sticky tapes, covered approximately 2–4 % of the total surface area of the apple. Two sensors of each type were used, and the average readings were taken for model predictions. The duration and amount of surface condensation were measured from experimental weighing balance mass and compared with model predictions of apple mass. The predicted-to-experimental ratio was determined as the ratio of the peak predicted condensation amount to the peak experimental condensation amount. It is then converted to a percentage to provide a clearer understanding of the accuracy of the prediction. Similarly, wetness signal data was also compared with the experimental retention time of surface condensation (Linke et al., 2021). The individual apple trials did not include the measurement of air speed, as the cooling chamber did not have an in-built fan to circulate air, and therefore, the air speed was assumed to be zero. Additionally, these experiments did not involve the measurement of the wetness signal.

3.2. IoT system

An earlier described digital twin platform (Jedermann et al., 2023) was expanded to include the necessary hardware components for sensor integration, forming an IoT-enabled platform (Fig. 2). Sensor data were initially collected and pre-processed on a microcontroller platform to convert binary raw data into physical values. The functions of each sensor and microcontroller are listed in Table 2. The STM32L031K Nucleo board was chosen for its affordability and low energy consumption, offering support for I^2C, eight analogue inputs, and USB connectivity.

The Nucleo boards were connected to a Raspberry Pi (RPi) via USB, with the RPi providing four USB inputs that can be extended using USB hubs. Acting as a bridge, the RPi forwarded sensor data to the Kafka streaming platform via Ethernet. The system was designed for scalability by adding additional Nucleo boards, with further RPis deployed if USB port availability became a limitation. The RN2483 radio module was used in these experiments for its reliable support of Lora-based communication, enabling the transmission of data over long distances with low power consumption.

3.3. Kafka streaming platform

The IoT platform used a Kafka-based streaming system to efficiently handle sensor data (Fig. 2). Each sensor was linked to a dedicated data stream, which served as an intermediate storage layer, allowing multiple services to subscribe and process the data as new packets became available. These services typically read data from one or more streams, perform specific operations such as calibration, resampling, or running models, and write the results back to a different stream (Jedermann et al., 2024). The system included a condensation and mass loss model developed in Section 2 as the primary data processing service.

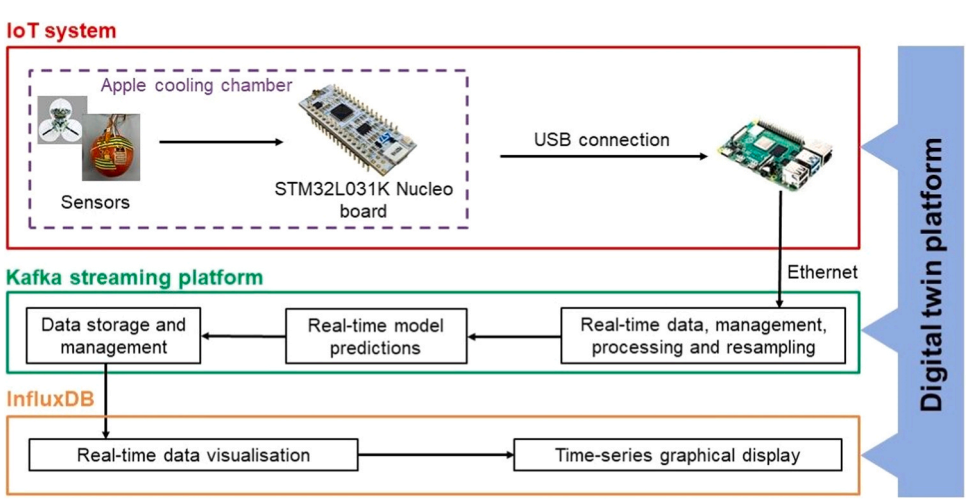

Fig. 2. Digital twin platform: an IoT system integrating Kafka streaming and InfluxDB for predictive modelling of condensation and mass loss in apples.

The sensor integration services ran on the RPi, reading measurements via USB and forwarding them to the data streams. Wireless sensors could also be integrated by substituting the data forwarding service, where the sensor data was collected from a compatible data collection unit and forwarded to the streams. Other services forwarded measurement data and predicted results to the graphical interface or CSV files for offline analysis.

The Kafka streaming platform (Kamath et al., 2020) ran on a virtual Linux server with four CPU cores and 8 GB of memory, and all services were implemented in Python. The system design allowed services to be distributed across multiple servers if CPU resources became a bottleneck.

3.4. Graphical display

InfluxDB is a database for time-series data. It offers a web-based interface for real-time data visualisation, as well as the capability to upload sensor and other data via the internet. However, it provides only limited support for integrating software services. Therefore, Kafka was used as the central database; InfluxDB was only applied as a graphical interface. The wetness sensor data, experimental balance mass of apples, and predicted cumulative condensation, retention time and mass loss were displayed in InfluxDB as outputs from the model.

4. Results and discussion

4.1. Real-time data

Figs. 3–6 show the temporal variations of air temperature, air relative humidity, apple surface temperature, cooling air speed, predicted parameters of dew point temperature, mass losses, cumulative condensation, cumulative mass loss and experimental apple mass for the four trials. The set operation cycle of the refrigeration systems in respective chambers caused cyclic fluctuations in temperature, facilitating sufficient cooling to induce mass loss from the apple and condensation on the apple surface as shown in Figs. 3**a**, 4**a**, 5**a** and 6**a**. The air relative humidity decreased during cooling phases and increased during warming periods. This behaviour is opposite to the typical air temperature and relative humidity observed in the atmosphere. This unusual phenomenon arose due to the limited volume of closed chambers, coupled with the evaporation of condensate and water from wet towels during the warming process, which increased the water vapour content in the air at higher temperatures. There was a correlation between air temperature, apple surface temperature, relative humidity, and dew point temperature, showcasing these factors as interdependent. The equilibrium between apple surface temperature and cooling air temperature occurred at a slower pace. Consequently, in the graphical representation, the apple surface temperature followed the trend of air temperature but with some time lag. This difference was attributed to the time required for the dense fruit structure to match the cooling temperature, resulting in a delayed resonance with the air temperature (Hoffmann et al., 2021). Figs. 3**b**, 4**b**, 5**b** and 6**c** display the predicted water content in the ambient air and the potential water content at the apple surface. The real-time predicted apple mass loss due to transpiration (Eq. (14)) and respiration (Eq. (15)), along with the summation of both (total mass loss), as well as the cumulative condensation (Eq. (8)) and mass loss, are illustrated in Figs. 3**c**, 4**c**, 5**c**, and 6**c**. The cumulative effect of condensation and mass loss (Eq. (16)) on the apple mass, referred to as the predicted apple mass along with experimental apple mass, is shown in Figs. 3**d**, 4**d**, 5**d**, and 6**d**.

Table 3 summarises the key model predictions from the four trials, highlighting the variations in air and apple surface water content, as well as dew point temperatures. In trial #1 (Fig. 3**b**, 45-minute on-off cycle), air water content ranged from 4.08 to 6.70 g m^{-3}, and apple surface water content from 5.30 to 6.03 g m^{-3}, with a dew point temperature between −2.1°C and 5.0°C. Trial #2 (Fig. 4**b**, 60-minute on-off

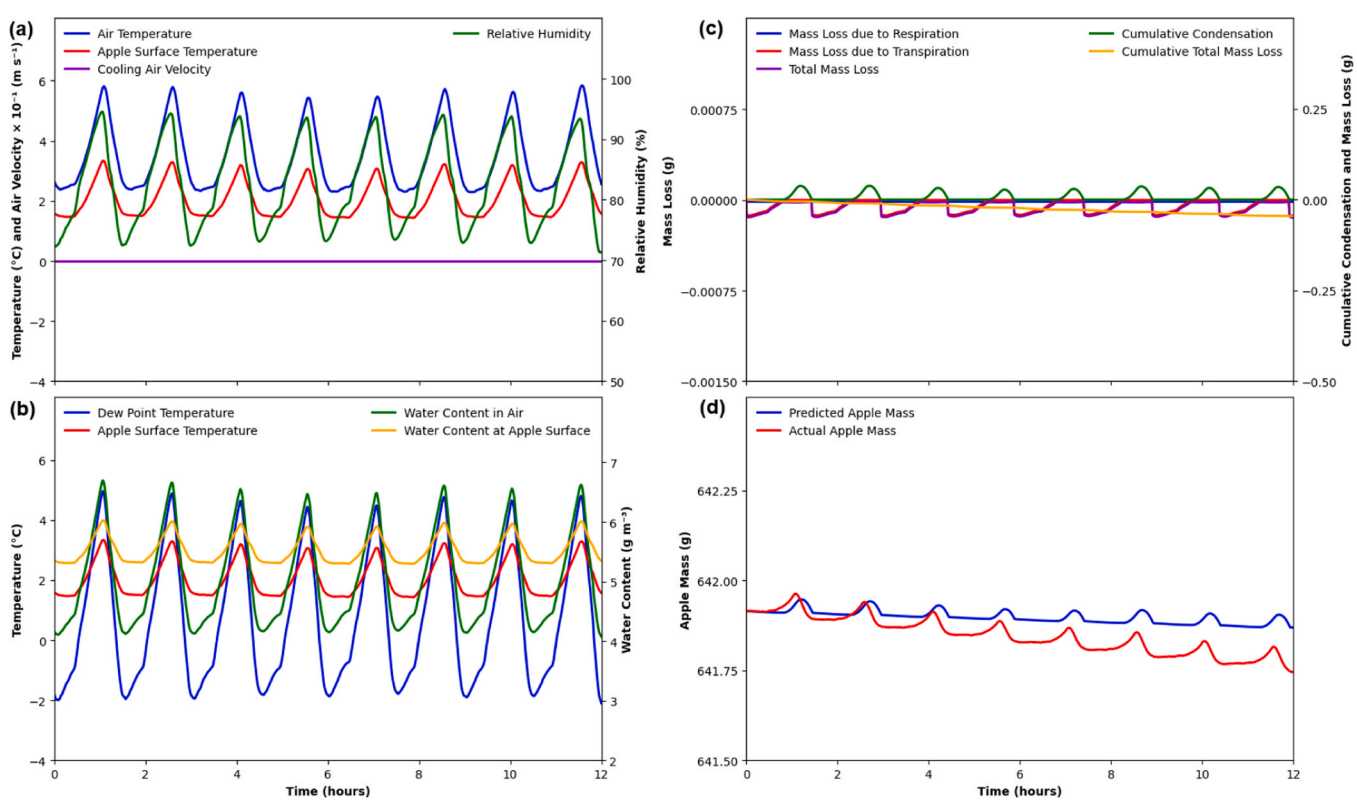

Fig. 3. Individual apple trial #1 under 45 minutes on-off refrigeration cycle: (a) Variations in temperature and cooling air speed; (b) Dew point temperature and water content in the air and at the surface of the apple; (c) Real-time predicted mass losses, cumulative condensation, and total mass loss; and (d) Model predicted and experimental apple mass over time.

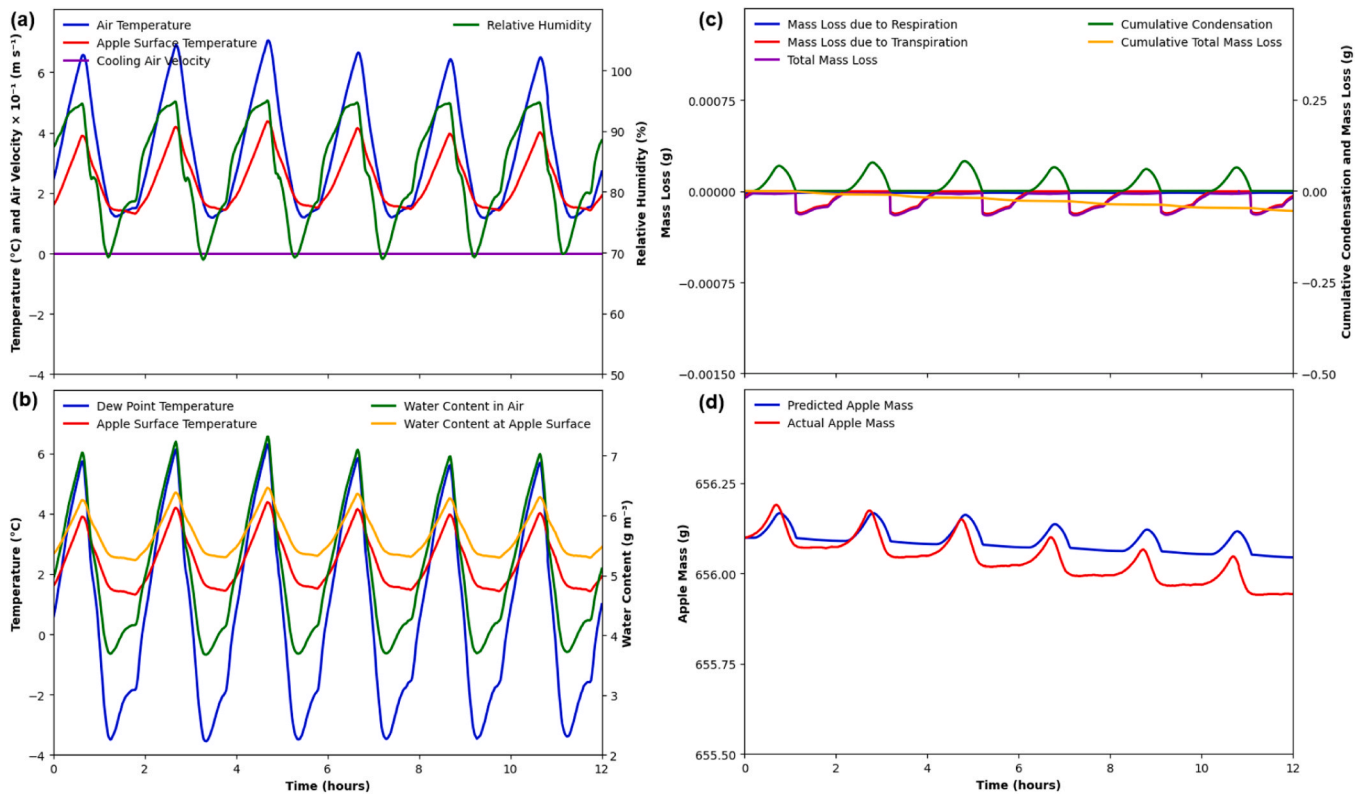

Fig. 4. Individual apple trial #2 under 60 minutes on-off refrigeration cycle: (a) Variations in temperature and cooling air speed; (b) Dew point temperature and water content in the air and at the surface of the apple; (c) Real-time predicted mass losses, cumulative condensation, and total mass loss; and (d) Model predicted and experimental apple mass over time.

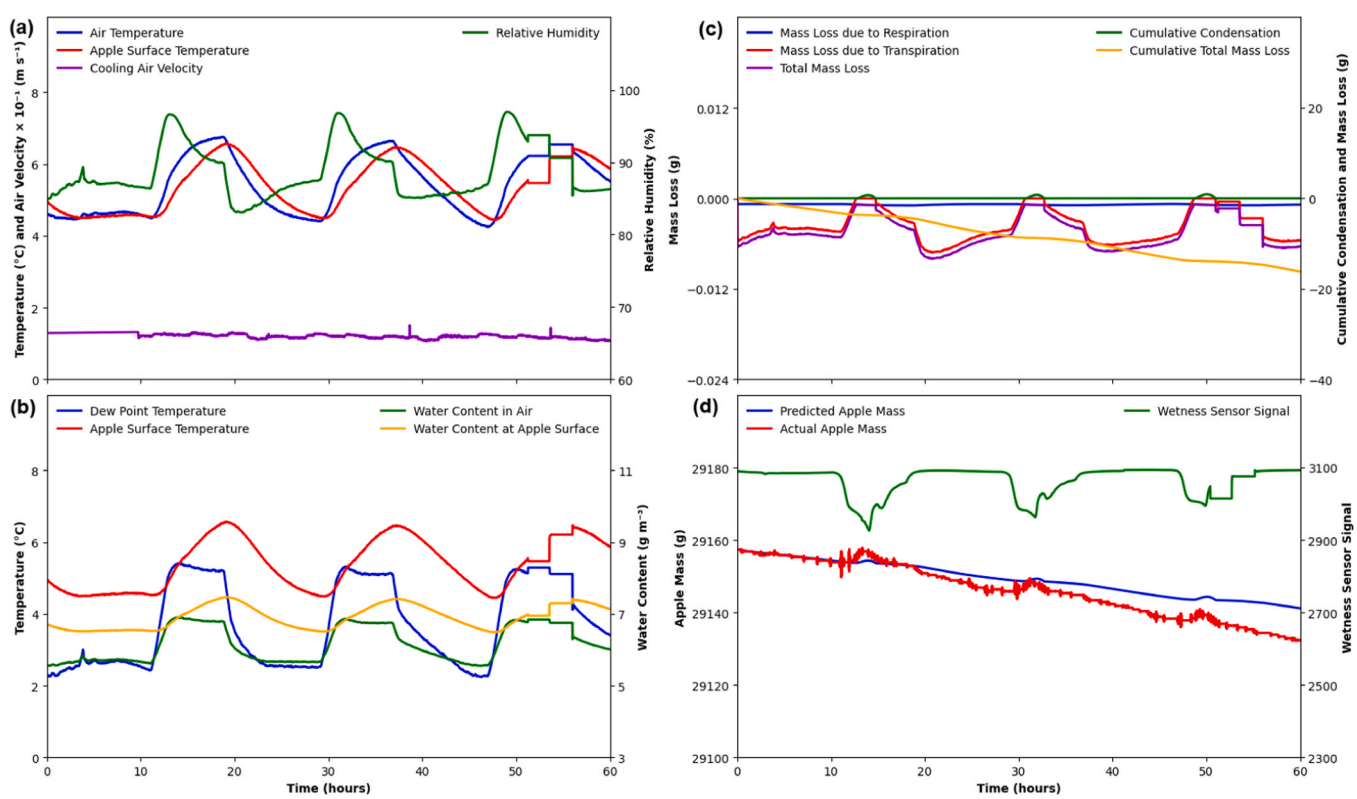

Fig. 5. Bulk apple trial #3 under low-temperature fluctuations: (a) Variations in temperature and cooling air speed; (b) Dew point temperature and water content in the air and at the surface of the apple; (c) Real-time predicted mass losses, cumulative condensation, and total mass loss; and (d) Wetness sensor signals, along with model predicted and experimental apple mass over time.

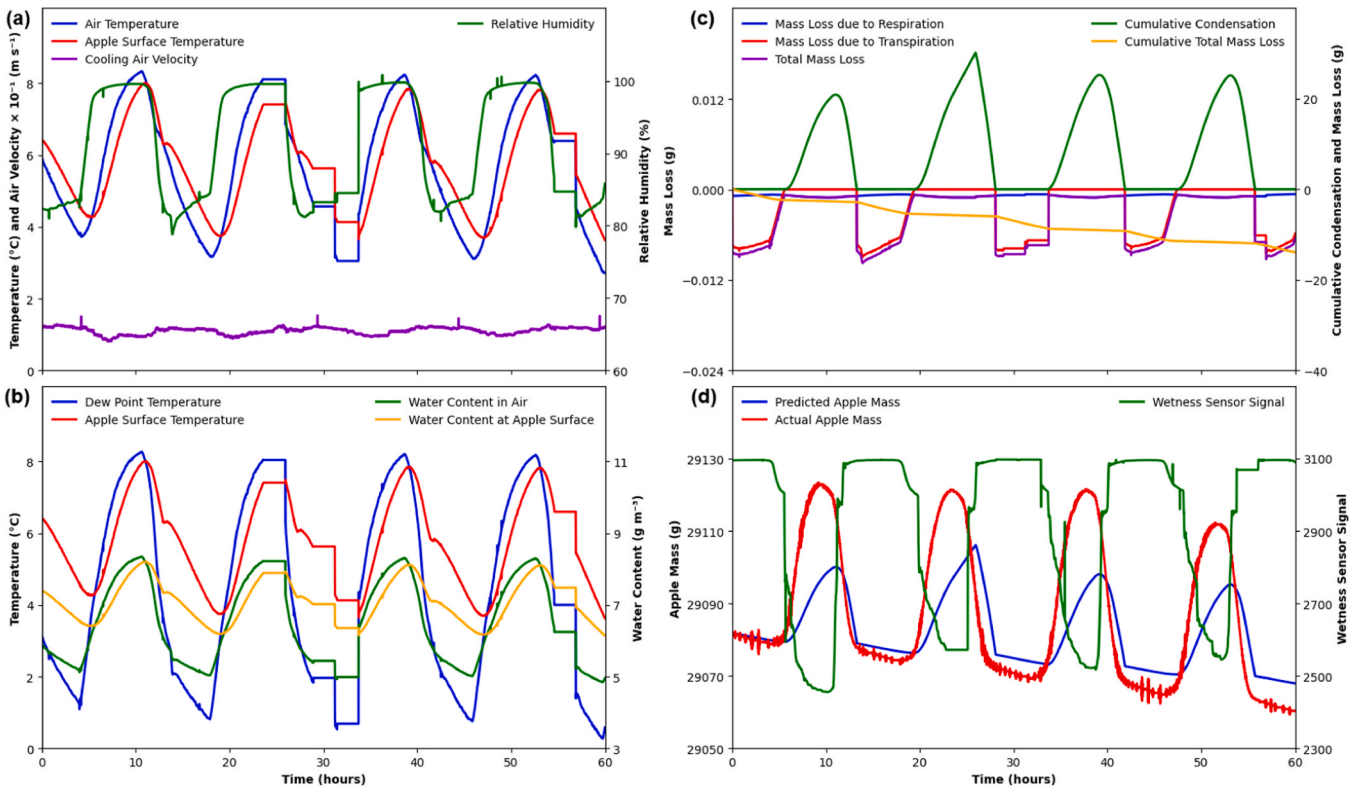

Fig. 6. Bulk apple trial #4 under high-temperature fluctuations: (a) Variations in temperature and cooling air speed; (b) Dew point temperature and water content in the air and at the surface of the apple; (c) Real-time predicted mass losses, cumulative condensation, and total mass loss; and (d) Wetness sensor signals, along with model predicted and experimental apple mass over time.

Table 3
Mass transfer coefficients, peak predicted vs. experimental cumulative condensation, and peak mass loss due to transpiration for each trial.

Trial number	Air water content (g m^{-3})	Apple surface water content (g m^{-3})	Dew Point Temperature (°C)	Mass transfer coefficient (m s^{-1})	Peak predicted real-time cumulative condensation (g kg^{-1})	Peak experimental real-time cumulative condensation (g kg^{-1})	Predicted versus experimental ratio (%)	Predicted peak real-time mass loss due to transpiration (g kg^{-1})
#1	4.1–6.7	5.3–6.0	−2.1–5.0	~1.20 × 10^{-3}	0.05	0.07	71	3.51 × 10^{-6}
#2	3.7–7.3	5.3–6.5	−3.5–6.3	~1.20 × 10^{-3}	0.12	0.15	77	2.71 × 10^{-6}
#3	5.6–6.9	6.5–7.5	2.2–5.4	5.66 × 10^{-3} to 6.55 × 10^{-3}	0.03	0.10	30	3.08 × 10^{-5}
#4	4.9–8.3	6.1–8.2	0.3–8.3	5.12 × 10^{-3} to 6.57 × 10^{-3}	1.03	1.80	58	3.29 × 10^{-5}

cycle) showed higher temperature fluctuations, with air water content ranging from 3.68 to 7.32 g m^{-3}, apple surface water content from 5.26 to 6.46 g m^{-3}, and dew point temperature between −3.5°C and 6.3°C. In trial #3 (Fig. 5**b**, lower temperature fluctuations), air water content ranged from 5.56 to 6.91 g m^{-3}, apple surface water content from 6.49 to 7.47 g m^{-3}, and dew point temperature varied between 2.2°C and 5.4°C. Trial #4 (Fig. 6**b**, higher temperature fluctuations) exhibited the widest variations, with air water content between 4.85 and 8.34 g m^{-3}, apple surface water content from 6.14 to 8.21 g m^{-3}, and dew point temperature ranging from 0.3°C to 8.3°C. The on-off cycle time (trials #1 and #2) and temperature fluctuations (trials #3 and #4) played a significant role in regulating the water content dynamics between the apple surface and the surrounding air. In particular, higher temperature fluctuations and longer on-off cycle times resulted in greater variation in both the air water content and apple surface water content. The large difference in maximum and minimum values of dew point temperature across all trials was observed compared to other measured temperatures, attributing to its dependency on both air relative humidity and temperature.

4.2. Amount of condensation

Figs. 3**c**, 4**c**, 5**c**, and 6**c** display the real-time predicted condensation amounts at 60-second intervals (primary axis) and the cumulative amounts (secondary axis) as positive values, reflecting their addition to the real-time apple mass. The range of predicted mass transfer coefficient for condensation, as shown in Table 3, varied across all trials, reflecting the influence of air velocities on the amount of condensation on the apple surface. The mass transfer coefficient remained constant (1.20 × 10^{-3} m s^{-1}) for trials #1 and #2, as the air speed was zero. In contrast, for trials #3 and #4, the mass transfer coefficients (5.66 × 10^{-3} to 6.55 × 10^{-3} m s^{-1} and 5.12 × 10^{-3} to 6.57 × 10^{-3} m s^{-1}) exhibited variability due to minor fluctuating air speeds around 0.1 m s^{-1}. A comparison of the peak real-time (60-second interval) predicted and experimental cumulative condensation values is highlighted in Table 3 with the predicted versus experimental ratios. In trial #1, the predicted cumulative condensation peaked at 0.04 g (0.05 g kg^{-1}), while the experimental peak was 0.07 g kg^{-1}. In trial #2, predicted condensation reached 0.08 g (0.12 g kg^{-1}), with an

experimental peak of 0.14 g kg^{-1}. For trial #3, the predicted cumulative condensation peaked at 0.87 g (0.03 g kg^{-1}), compared to an experimental peak of 0.10 g kg^{-1}. In trial #4, predicted condensation peaked at 30.16 g (1.03 g kg^{-1}), while the experimental peak was 1.83 g kg^{-1}. In individual apple trials, the predicted values closely matched the experimental data (Figs. 3**d** and 4**d**), with predicted-to-experimental ratios of 71 % and 77 %, respectively. However, larger deviations were observed in bulk apple trials, where the predicted-to-experimental ratios were 30 % and 58 %, respectively (Figs. 5**d** and 6**d**). This discrepancy may be attributed to other surfaces, such as the weighing balance plate, sensor wiring, and the box, all of which also experienced condensation on their surfaces but were not considered in the calculation of cumulative condensation. Conversely, the calculation of the mass transfer coefficient, derived from the Sherwood number, relied solely on theoretical mathematical equations. This difference can introduce the potential for inaccuracies in predicting condensation amounts. Additionally, the real-time predicted condensation showed a slight delay (8 seconds from the SHT45 sensor) compared to the experimental values, which could be due to the response time of sensors in adjusting to changes in environmental conditions. Ultimately, the model predictions for cumulative condensation amounts (Figs. 3**c**, 4**c**, 5**c** and 6**c**) closely followed the experimental trend in all trials, though not perfectly in numerical terms, but aligned well in graphical representation (Figs. 3**d**, 4**d**, 5**d** and 6**d**).

In a study conducted by Linke et al. (2021), it was observed that condensation on an apple peaked at around roughly 2.09 g kg^{-1} of apple surface area. Lequentrec et al. (2023) noticed uneven condensation and evaporation under air speed (0.33 m s^{-1}). The front surface of the orange fruit-facing air speed warmed up faster than the rear, leading to faster evaporation at the front while condensation continued at the rear. However, in the current study, it was assumed that condensation was evenly distributed on the apple surface. This would be interesting to investigate the condensation at different apple surfaces and the total wetness area of apples considering the direction of cooling airflow. The studies for the condensation model in literature did not predict the real-time condensation dynamics nor did it account for lower and higher fluctuations to check the robustness of the model in bulk of fruits. Real-time condensation dynamics, as demonstrated in this study, facilitate timely decision-making, enhance resource optimisation, and promote better integration within operational frameworks.

4.3. Condensation retention time

Fig. 7 illustrates the comparison between the predicted and experimental retention times and the corresponding mass loss over time across different trial conditions. In trials #1 and #2, with individual apple trials, the model predictions of condensate retention times were very close to the experimental data, with minor deviations. This suggests that the model performs well in individual apple trials, accurately predicting the presence of condensate and the resulting mass loss. However, in bulk apple trials (#3 and #4), the model showed more significant deviations, especially in trial #4. The experimental retention time for trial #3 showed a larger discrepancy, indicating that the model may struggle more with larger apple quantities or environments with greater fluctuations. The predictions of the IoT model were based on dew point undershoot techniques. The underestimation of condensation retention time in trial #3 and overestimation in trial #4 may be attributed to the limitations of the model in accounting for rapid changes in temperature, humidity, and air speed, especially during higher fluctuations. In contrast, the wetness signal appeared more sensitive to smaller fluctuations (trial #3) and the increased humidity in the environment, leading to a slightly better prediction of condensation retention time than higher fluctuation (trial #4) in bulk apple trials (Figs. 5**d** and 6**d**). In trial #3, the percentage deviations from experimental values for the predicted retention time and the wetness sensor signal retention time were 12.61 % and 10.30 %, respectively. In trial #4, the percentage deviations from experimental values for the predicted retention time and the wetness sensor signal retention time were 3.64 % and 21.40 %, respectively. In trial #1, the model predicted condensate presence for 40.97 % of the total time, while in trial #2, the prediction was 46.39 %. For the bulk apple trials, trial #3 predicted 10.61 % of the total time with condensate presence, while trial #4 predicted 53.83 % of the total

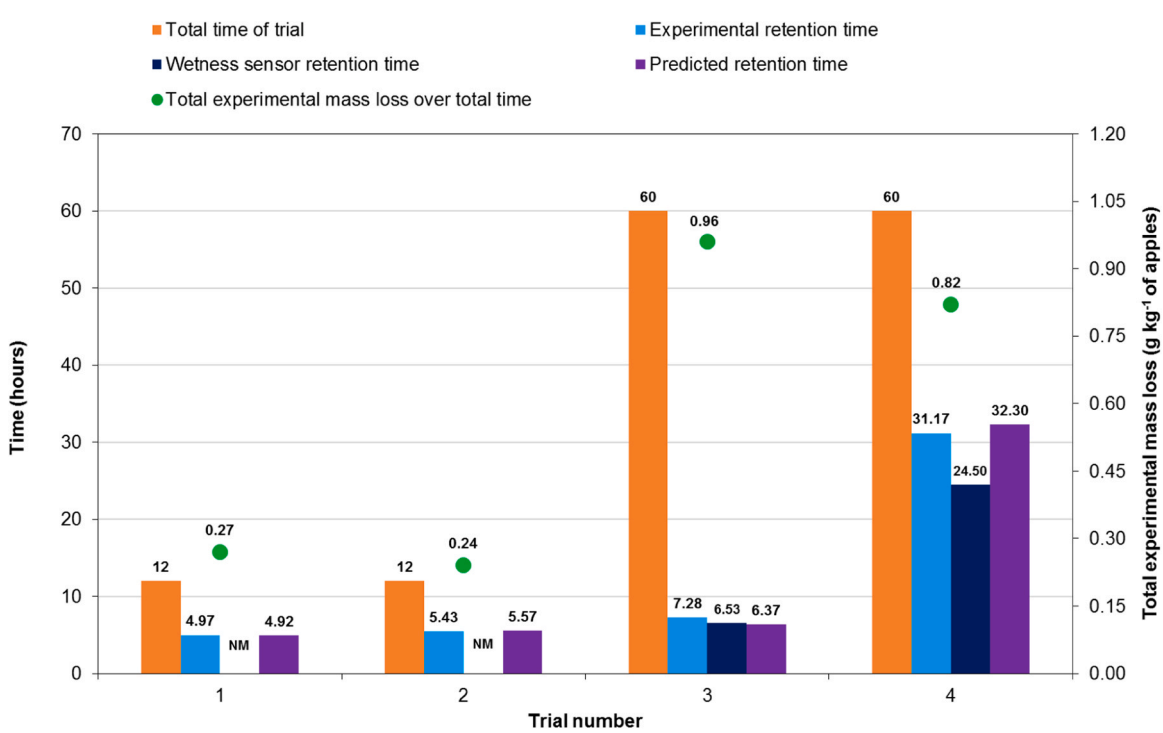

Fig. 7. Comparison of experimental, wetness sensor and model predicted condensation (presence) retention times and mass loss in apple trials, highlighting the percentage of condensate retention and cumulative mass loss for each trial. NM indicates data points that were not measured.

time. Thus, trials #2 and #4, with higher temperature fluctuations, led to more condensation on the apple surface, resulting in increased condensation presence or retention time.

Linke et al. (2023) reported that the dew point undershoot measurements predicted shorter retention times than the wetness sensor. However, the actual weighing balance measurements were not carried out to compare with wetness and dew point undershoot measurements. In this study, the wetness sensor was effective in measuring condensation retention time. Similarly, Lequentrec et al. (2023) used wetness sensors on oranges, finding that both experimental and predicted retention times closely aligned with the wetness signal, though evaporation times varied between the front and rear of the fruit. The use of wetness sensors can increase the cost of continuous operation, including electricity expenses. Additionally, wetness sensors may become damaged or prone to failure when exposed to high moisture levels. Consequently, predictive models are a better alternative, though they sometimes show slight under- or overestimations compared to actual retention times. Lequentrec et al. (2023) emphasised that the retention time of condensation, rather than the quantity, is a key factor affecting the quality of fresh produce. When no condensation occurs, it means that the refrigeration system operates at full capacity with constant temperature (without no-off cycle), which can lead to water loss from fresh produce due to water vapour pressure difference. This water loss can lead to degrade the quality of fruit, affecting its texture, nutritional value, and overall freshness. For produce like apples, reducing mass through water loss can result in reduced shelf life and lower consumer acceptance due to shrivelling or nutrient degradation (Ziv and Fallik, 2021).

4.4. Mass loss from apples

Figs. 3**c**, 4**c**, 5**c**, and 6**c** present all predicted mass losses at 60-second intervals (primary axis), alongside the cumulative total mass loss (secondary axis) as negative values, signifying a reduction from the initial apple mass. Each time condensate evaporation was completed, transpirational mass loss resumed. Table 3 presents the peak real-time (60-second intervals) mass loss due to transpiration across all the trials. Trials #3 and #4 exhibited higher peaks of real-time mass loss due to transpiration, likely due to the higher air velocities in these trials, which resulted in an increased mass transfer coefficient for transpiration than trials #1 and #2. The oxidative mass loss (60-second interval) was equal to total mass when there was condensate present on the apple surface, therefore the purple line (total mass loss) overlaps with the blue line (mass loss due to respiration) when condensation is present on the apple surface as seen in Figs. 3**c**, 4**c**, 5**c**, and 6**c**. In individual apple trials, oxidative mass loss was nearly zero and consistent, causing the purple line (total mass loss) to overlap with the red line (mass loss due to transpiration) in Figs. 3**c** and 4**c**. In bulk apple trials, oxidative mass loss was minimal and consistent, having little impact on the total mass loss, as shown in Figs. 5**c** and 6**c**. This small oxidative loss resulted from the natural respiration of apples, which remained stable since temperatures did not exceed 10°C in either experimental trial. The total experimental mass loss over the total time of each trial is shown in Fig. 7. Over 12 hours, the total experimental mass loss in trial #1 was 0.17 g (0.27 g kg^{-1} of apples), and in trial #2, it was 0.16 g (0.24 g kg^{-1}) for apples weighing ~0.6 kg. Over 60 hours, trial #3 showed a mass loss of 27.80 g (0.96 g kg^{-1}), while trial #4 recorded 23.70 g (0.82 g kg^{-1}) for ~29 kg of apples. This reduction, driven primarily by transpiration with minor oxidation, closely matched predictions from the real-time model. The results indicated that higher fluctuations in temperature (trials #2 and #4) led to longer condensation times, resulting in lower cumulative mass loss compared to the low-fluctuation conditions (trials #1 and #3), which had shorter condensation times. The increased condensation presence time in trials #2 and #4 for the respective apple experiment, despite the higher temperature fluctuations, contributed to a reduction in cumulative total mass loss as transpiration was zero during condensation time. Condensation on apple surfaces, while often seen as an indicator of excess moisture, can serve a beneficial role in reducing overall mass loss by minimising transpirational mass loss. This is because when condensation is present on the apple surface, it acts as a barrier, slowing down the loss of internal water vapour from the fruit into the surrounding air. As a result, transpiration, the main process responsible for the mass loss, is temporarily suppressed during periods of surface condensation (Jalali et al., 2020; Shrivastava et al., 2023). The total model-predicted mass loss from apples was 0.08, 0.08, 0.58, and 0.48 g kg^{-1} for trials #1, #2, #3, and #4, respectively, over the duration of their respective experiments. These predicted values are significantly lower than the experimental values, being approximately one-third for trials #1 and #2, and about half for trials #3 and #4. However, the model predictions for cumulative total mass loss (Figs. 3**c**, 4**c**, 5**c**, and 6**c**) closely aligned with the experimental trends observed in all trials (Figs. 3**d**, 4**d**, 5**d**, and 6**d**).

Over a six-month storage period, the simulated mass loss for the individual apple trials was 9.7 % under a 45-minute on-off cycle and 8.4 % under a 60-minute on-off cycle. For the bulk apple, the simulated mass loss was 6.3 % under low-temperature fluctuations and 5.9 % under high fluctuations. These calculations assumed a constant rate of mass loss over six months; however, in reality, the rate of mass loss gradually decreases over time. As a result, the predicted values are slightly higher than those typically reported in the literature. Nonetheless, these results are plausible given the range of temperature and relative humidity fluctuations considered in the study.

The model predictions showed some differences from the experimental values. It used several temperature-dependent numerical parameters (respiration rate of apple, density, thermal conductivity, viscosity, diffusivity, and the specific heat capacity of humid air) from the literature, which can be adjusted through numerical calculations to better match the experimental results. In this study, measurements were conducted at a single data point, but temperature and air speed distributions are unlikely to be uniform across the entire experimental region. Therefore, spatial distribution analysis could be performed in future studies to investigate the condensation behaviour at each specific spot or microenvironment surrounding the apples (Jedermann and Lang, 2009). This approach would provide a more accurate understanding of how local variations in environmental conditions impact condensation patterns. Conducting a model uncertaninty through model parameter variability analysis is essential to assess the robustness of the model and identify the key variables that significantly influence the outcomes. For futuristic goals, this IoT model can be seamlessly integrated into a digital twin platform (Fig. 2) with real-time feedback and interventions using model predictions in the cooling chamber through the refrigeration cycle. Thus, optimising the refrigeration cycle based on real-time data improves control over condensation and evaporation processes, reducing condensation-related diseases, minimising energy consumption, and increasing overall efficiency. By simulating real-time environmental conditions and predicting condensation and mass loss dynamics, the digital twin can provide insights for fine-tuning storage environments and minimising energy consumption while increasing shelf life.

5. Conclusions

- The IoT model demonstrated real-time predictive ability with condensation, retention time, and mass loss dynamics across varying temperature fluctuations. The IoT model could match the trends of experimental values, showing its reliability in extreme temperature fluctuation conditions.
- The model underestimated peak condensation amount compared to experimental results. The predicted-to-experimental peak condensation ratio was 71 % and 77 % for individual apple trials, 30 % for low-temperature fluctuations in bulk trials, and 58 % for high fluctuations in bulk trials.

- Notably, high fluctuations in air temperature (60 minutes on-off cycle trial of individual apples and high-temperature fluctuation trial of bulk apples) led to significantly greater cumulative condensation amount. The predicted apple mass loss accurately followed the experimental values, demonstrating that the predictive model for mass loss is effective, especially when compared to the condensation amounts.
- The difference between all experimental and predicted values likely could result from sensor accuracy, the complexity of the experimental setup, and assumptions in the theoretical model. Additionally, a longer surface condensation retention time resulted in less apple mass loss. Condensation on the apple surface acted as a barrier to transpiration mass loss, resulting in reduced overall mass loss from apples.
- The predictive accuracy of the IoT model suggests that it could be integrated into a digital twin platform for real-time monitoring and optimisation of refrigeration systems, potentially enhancing energy efficiency and prolonging fruit shelf life.

Funding

This work was supported by the Deutsche Forschungsgemeinschaft (DFG, German Research Foundation) project Fruity-Twin (Project number: 521409147).

CRediT authorship contribution statement

Sonawane Akshay D.: Writing – original draft, Visualization, Validation, Software, Methodology, Investigation, Formal analysis, Data curation, Conceptualization. **Hoffmann Tuany G.:** Writing – review & editing, Validation, Methodology, Investigation, Data curation. **Jedermann Reiner:** Writing – review & editing, Validation, Software, Methodology, Funding acquisition, Conceptualization. **Linke Manfred:** Writing – review & editing, Supervision. **Mahajan Pramod V.:** Writing – review & editing, Supervision, Resources, Project administration, Methodology, Funding acquisition, Conceptualization.

Declaration of Competing Interest

There is no conflict of interest.

Appendix A. Supporting information

Supplementary data associated with this article can be found in the online version at doi:10.1016/j.postharvbio.2025.113520.

Data availability

Data will be made available on request.

References

Becker, B.R., Misra, A., Fricke, B.A., 1996. Bulk refrigeration of fruits and vegetables Part I: theoretical considerations of heat and mass transfer. HVACR Res. 2, 122–134. https://doi.org/10.1080/10789669.1996.10391338.

Bovi, G.G., Caleb, O.J., Linke, M., Rauh, C., Mahajan, P.V., 2016. Transpiration and moisture evolution in packaged fresh horticultural produce and the role of integrated mathematical models: a review. Biosyst. Eng. 150, 24–39. https://doi.org/10.1016/j.biosystemseng.2016.07.013.

Bovi, G.G., Caleb, O.J., Rauh, C., Mahajan, P.V., 2019. Condensation regulation of packaged strawberries under fluctuating storage temperature. Packag. Technol. Sci. 32, 545–554. https://doi.org/10.1002/pts.2470.

Chen, Y., Xing, M., Chen, T., Tian, S., Li, B., 2023. Effects and mechanisms of plant bioactive compounds in preventing fungal spoilage and mycotoxin contamination in postharvest fruits: a review. Food Chem. 415, 135787. https://doi.org/10.1016/j.foodchem.2023.135787.

Clayton, M., Amos, N.D., Banks, N.H., Morton, R.H., 1995. Estimation of apple fruit surface area. N. Z. J. Crop Hortic. Sci. 23, 345–349. https://doi.org/10.1080/01140671.1995.9513908.

Defraeye, T., Shrivastava, C., Berry, T., Verboven, P., Onwude, D., Schudel, S., Bühlmann, A., Cronje, P., Rossi, R.M., 2021. Digital twins are coming: will we need them in supply chains of fresh horticultural produce? Trends Food Sci. 109, 245–258. https://doi.org/10.1016/j.tifs.2021.01.025.

Geyer, M., Praeger, U., Truppel, I., Scaar, H., Neuwald, D.A., Jedermann, R., Gottschalk, K., 2018. Measuring device for air speed in macroporous media and its application inside apple storage bins. Sensors 18, 576. https://doi.org/10.3390/s18020576.

Gottschalk, K., Linke, M., Mészáros, C., Farkas, I., 2007. Modeling condensation and evaporation on fruit surface. Dry. Technol. 25, 1237–1242. https://doi.org/10.1080/07373930701438667.

Hoffmann, T.G., Linke, M., Praeger, U., Sonawane, A.D., Büchele, F., Neuwald, D.A., Jedermann, R., Sturm, B., Mahajan, P.V., 2024. Heat transfer in large bins during the apples cool-down process. Int. J. Refrig. 170, 60–69. https://doi.org/10.1016/j.ijrefrig.2024.11.023.

Hoffmann, T.G., Ronzoni, A.F., da Silva, D.L., Bertoli, S.L., de Souza, C.K., 2021. Impact of household refrigeration parameters on postharvest quality of fresh food produce. J. Food Eng. 306, 110641. https://doi.org/10.1016/j.jfoodeng.2021.110641.

Huang, J., 2018. A simple accurate formula for calculating saturation vapor pressure of water and ice. J. Appl. Meteorol. Climatol. 57, 1265–1272. https://doi.org/10.1175/JAMC-D-17-0334.1.

Huang, W., Wang, X., Zhang, J., Xia, J., Zhang, X., 2023. Improvement of blueberry freshness prediction based on machine learning and multi-source sensing in the cold chain logistics. Food Control 145, 109496. https://doi.org/10.1016/j.foodcont.2022.109496.

Incropera, F., DeWitt, D., Bergman, T., Lavine, A., 2007. Fundamentals of Heat and Mass Transfer. Fundamentals of Heat and Mass Transfer, Sixth ed. John Wiley & Sons, Hoboken, NJ (USA).

Jalali, A., Linke, M., Geyer, M., Mahajan, P., 2021. Integrative programming for simulation of packaging headspace and shelf life of fresh produce. MethodsX 8, 101514. https://doi.org/10.1016/j.mex.2021.101514.

Jalali, A., Linke, M., Geyer, M., Mahajan, P.V., 2020. Shelf life prediction model for strawberry based on respiration and transpiration processes. Food Packag. Shelf 25, 100525. https://doi.org/10.1016/j.fpsl.2020.100525.

Jedermann, R., Borysov, M., Hartgenbusch, N., Jaeger, S., Sellwig, M., Lang, W., 2018. Testing Lora for food applications-Example application for airflow measurements inside cooled warehouses with apples. Procedia Manuf. 24, 284–289. https://doi.org/10.1016/j.promfg.2018.06.026.

Jedermann, R., Hoffmann, T.G., Sonawane, A.D., Mahajan, P.V., Lüssem, B., 2024. Fruity Twin–A digital platform for processing sensor data in food cool chains. IEEE Sens. 1–4. https://doi.org/10.1109/SENSORS60989.2024.10785038.

Jedermann, R., Lang, W., 2009. The minimum number of sensors–Interpolation of spatial temperature profiles in chilled transports, Wireless Sensor Networks: 6th European Conference, EWSN 2009, Cork, Ireland, February 11-13, 2009. Proceedings 6. Springer, pp. 232–246. https://doi.org/10.1007/978-3-642-00224-3_15.

Jedermann, R., Singh, K., Lang, W., Mahajan, P., 2023. Digital twin concepts for linking live sensor data with real-time models. J. Sens. Sens. Syst. 12, 111–121. https://doi.org/10.5194/jsss-12-111-2023.

Kamath, V., Morgan, J., Ali, M.I., 2020. Industrial IoT and Digital Twins for a Smart Factory: An open source toolkit for application design and benchmarking, global internet of things summit (GIoTS), 2020. IEEE, pp. 1–6..

Kasera, R.K., Gour, S., Acharjee, T., 2024. A comprehensive survey on IoT and AI based applications in different pre-harvest, during-harvest and post-harvest activities of smart agriculture. Comput. Electron. Agric. 216, 108522. https://doi.org/10.1016/j.compag.2023.108522.

Lequentrec, G., Chaomuang, N., Sambou, P., Alvarez, G., Flick, D., Duret, S., 2023. Experimental and modelling study of water condensation and evaporation at the surface of fruits during cold chain breaks, 26th International Congress of Refrigeration ICR 2023. 〈https://hal.science/hal-04231593#:~:text=This%20study%20presents%20the%20evolution%20of%20the%20quantity,following%20storage%20at%20low%20temperature%20and%20high%20humidity〉.

Li, T., Zhou, J., Liu, R., Yuan, Z., Li, J., 2022. Effects of photo-selective nets and air humidity coupling on tomato resistance to Botrytis cinerea. Sci. Hortic. 305, 111356. https://doi.org/10.1016/j.scienta.2022.111356.

Linke, M., Geyer, M., 2013. Condensation dynamics in plastic film packaging of fruit and vegetables. J. Food Eng. 116, 144–154. https://doi.org/10.1016/j.jfoodeng.2012.11.026.

Linke, M., Hoffmann, T.G., Sonawane, A.D., Rux, G., Mahajan, P.V., 2024. Method for measuring the transpiration resistance of fruit and vegetables. MethodsX 13, 103058. https://doi.org/10.1016/j.mex.2024.103058.

Linke, M., Praeger, U., Mahajan, P.V., Geyer, M., 2021. Water vapour condensation on the surface of bulky fruit: some basics and a simple measurement method. J. Food Eng. 307, 110661. https://doi.org/10.1016/j.jfoodeng.2021.110661.

Linke, M., Praeger, U., Neuwald, D.A., Geyer, M., 2023. Measurement of water vapor condensation on apple surfaces during controlled atmosphere storage. Sensors 23, 1739. https://doi.org/10.3390/s23031739.

Lufu, R., Ambaw, A., Opara, U.L., 2019. The contribution of transpiration and respiration processes in the mass loss of pomegranate fruit (cv. Wonderful). Postharvest Biol. Technol. 157, 110982. https://doi.org/10.1016/j.postharvbio.2019.110982.

Magnus, G., 1844. Versuche über die Spannkräfte des Wasserdampfs. Ann. Phys. 137, 225–247.

Montgomery, R., 1947. Viscosity and thermal conductivity of air and diffusivity of water vapor in air. J. Atmos. Sci. 4, 193–196. https://doi.org/10.1175/1520-0469(1947)004< 0193:VATCOA> 2.0.CO;2.

Paull, R., 1999. Effect of temperature and relative humidity on fresh commodity quality. Postharvest Biol. Technol. 15, 263–277. https://doi.org/10.1016/S0925-5214(98)00090-8.

Praeger, U., Linke, M., Neuwald, D.A., Geyer, M., 2021. Water condensation on fruit surfaces during apple storage. IV Int. Symp. . Hortic. Eur. -SHE2021 1327, 591–596. https://doi.org/10.17660/ActaHortic.2021.1327.78.

Ramos, A.V., Sousa-Gallagher, M.J., Oliveira, J.C., 2023. Dimensionless correlations for estimating the permeability of perforated packaging films to oxygen. J. Food Eng. 340, 111252. https://doi.org/10.1016/j.jfoodeng.2022.111252.

Saquet, A.A., Streif, J., 2017. Respiration rate and ethylene metabolism of 'Jonagold' apple and 'Conference' pear under regular air and controlled atmosphere. Bragantia 76, 335-344. https://doi.org/10.1590/1678-4499.189.

Sensirion, 2024. SHT45 - Digital humidity and temperature sensor datasheet. ⟨https://sensirion.com/products/catalog/SHT45⟩ (accessed 01 September 2024).

Shoji, K., Schudel, S., Shrivastava, C., Onwude, D., Defraeye, T., 2022. Optimizing the postharvest supply chain of imported fresh produce with physics-based digital twins. J. Food Eng. 329, 111077. https://doi.org/10.1016/j.jfoodeng.2022.111077.

Shrivastava, C., Schudel, S., Shoji, K., Onwude, D., da Silva, F.P., Turan, D., Paillart, M., Defraeye, T., 2023. Digital twins for selecting the optimal ventilated strawberry packaging based on the unique hygrothermal conditions of a shipment from farm to retailer. Postharvest Biol. Technol. 199, 112283. https://doi.org/10.1016/j.postharvbio.2023.112283.

Sonawane, A.D., Chaiwong, S., Weltzien, C., Mahajan, P.V., 2024. A model integrating fruit physiology, perforation, and scavenger for prediction of ethylene accumulation in fruit package. Postharvest Biol. Technol. 209, 112734. https://doi.org/10.1016/j.postharvbio.2023.112734.

STMicroelectronics, 2024. STM32L031K6 microcontroller. ⟨https://www.st.com/en/microcontrollers-microprocessors/stm32l031k6.html⟩ (accessed 13 September 2024).

Veraverbeke, E.A., Verboven, P., Van Oostveldt, P., Nicolaı, B.M., 2003a. Prediction of moisture loss across the cuticle of apple (Malus sylvestris subsp. Mitis (Wallr.)) during storage: part 1. Model development and determination of diffusion coefficients. Postharvest Biol. Technol. 30, 75–88. https://doi.org/10.1016/S0925-5214(03)00083-8.

Veraverbeke, E.A., Verboven, P., Van Oostveldt, P., Nicolaï, B.M., 2003b. Prediction of moisture loss across the cuticle of apple (Malus sylvestris subsp. mitis (Wallr.)) during storage: part 2. Model simulations and practical applications. Postharvest Biol. Technol. 30, 89–97. https://doi.org/10.1016/S0925-5214(03)00082-6.

Vicent, V., Ndoye, F., Verboven, P., Nicolaï, B., Alvarez, G., 2018. Quality changes kinetics of apple tissue during frozen storage with temperature fluctuations. Int. J. Refrig. 92, 165–175. https://doi.org/10.1016/j.ijrefrig.2018.05.023.

Wei, Y.Q., Bailey, B.J., Wilkinson, D., Lockwood, A., Stenning, B.C., 1998. Detecting surface condensation on tomato plants in greenhouse. Acta Hortic. 421, 57–64. https://doi.org/10.17660/ActaHortic.1998.421.4.

Ziv, C., Fallik, E., 2021. Postharvest storage techniques and quality evaluation of fruits and vegetables for reducing food loss. Agronomy 6, 1133. https://doi.org/10.3390/agronomy11061133.